RC23099 (W0402-008) February 2, 2004
Materials Science

IBM Research Report

Structural and Surface Potential Characterization of Annealed HfO_2 and $(HfO_2)_x(SiO_2)_{1-x}$ Films

R. Ludeke, E. Gusev
IBM Research Division
Thomas J. Watson Research Center
P.O. Box 218
Yorktown Heights, NY 10598

Research Division
Almaden - Austin - Beijing - Haifa - India - T. J. Watson - Tokyo - Zurich

Structural and Surface Potential Characterization of Annealed HfO_2 and $(HfO_2)_x(SiO_2)_{1-x}$ films

R. Ludeke and E. Gusev
IBM T. J. Watson Research Center, P.O. Box 218, Yorktown Heights, NY 10598

***Abstract**:* The evolution on a microscopic scale of the surface morphology and contact potential differences (CPD) with high temperature anneals in ultra high vacuum to beyond the crystallization temperatures is reported for amorphous, as-grown 3 nm thick HfO_2 and 2.2 nm thick $Hf_{0.78}Si_{0.22}O_2$ layers on Si(100). The films were grown ex situ by atomic layer deposition and metal organic vapor deposition, respectively. A non-contact atomic force microscope operating in the electrostatic force mode was used to image the topography, surface potential and differential capacitance. The as-grown and annealed films essentially retained their smoothness even after undergoing crystallization; rms roughness of ~0.13 nm for HfO_2 and 0.077 nm for the 900° C annealed $Hf_{0.78}Si_{0.22}O_2$ layer were measured. These values compare favorably with state-of-the-art RTO and nitrided SiO_2 gate oxides. CPD fluctuations of up to 0.3-0.4 V were measured for 200x200 nm ^{2} images, values that did not change appreciably with annealing. A lack of correlation between topographic and CPD image features for the as-grown amorphous samples changed dramatically once the films crystallized, with higher CPD values associated with grain boundaries for both oxide and silicate layers. CPD variations were about a factor of two larger than for SiO_2 gate oxides. Differential capacitance images reflected mainly topographic surface features, as the high-κ inhibits image contrast in the images for small to moderate changes in κ. . Nevertheless, for the $Hf_{0.78}Si_{0.22}O_2$ sample annealed at 900° C, which exhibited the lowest roughness, increases in differential capacitance could be attributed to microstructures of high-κ material, most likely HfO_2, which phase separated during the anneal. Because of screening, the high κ dielectric also tends to suppress oxide charge contributions to the CPD image. A spherical tip model is presented that supports these observations.

1. Introduction

The quest for a high dielectric constant (κ) replacement of SiO_2 gate oxides has recently been focused predominantly on Hf (and to a lesser extent Zr) oxides and their more complex silicates and aluminates.[1-3] In general the pure binary oxides exhibit a higher κ, but are subject to crystallization when heated above 500-600° C, temperatures deemed rather moderate in conventional integrated circuit processing. Problems resulting from crystallization, which are primarily attributed to the formation of grain boundaries between crystallites, include enhanced diffusion, charge trapping, enhanced surface roughness with consequential larger thickness fluctuations and dielectric constant fluctuations. A further issue is that of workfunction (surface potential) variations due to the different grain orientations. Although efforts have been reported to raise the crystallization temperature by incorporating aluminum oxide or SiO_2, for example,[4] the unadulterated oxide would still be preferable provided that consequences of crystallization detrimental to device performance, a largely unknown issue, can be properly assessed and controlled if needed. In this paper we want to address some of these concerns on a microscopic scale, namely the role of crystallization on surface topography or roughness, the extent of surface potential fluctuations and its correlation with the topography, as well as possible variations in the dielectric constant due to material inhomogeneities. The technique used in these studies was non-contact Atomic Force Microscopy[5] (NC-AFM) and its variants Electric Force Microscopy, which under various names of Scanning Kelvin Probe Microscopy or Contact Potential Difference (CPD) Microscopy images the potential variations of the sample simultaneously with the AFM topography.[6-7] In addition differential capacitance imaging was used to evaluate annealed and phase-separated hafnium silicate layers. Due to the high dielectric constants of the layers, the AFM tip-surface interaction had to be modeled in order to evaluate the source of image contrast

in both the CPD and differential capacitance images. The model is developed in the next section, which also details the experimental setup and sample preparation. Section 3 discusses the structural and CPD changes of annealed HfO_2, whereas those for the annealed hafnium silicate, chosen for its interesting phase separated microstructure,[8] are discussed in section 4. A summary and final remarks are presented in section 5.

2. Sample preparation and experimental details.

Two different samples were used. A 3nm HfO_2 layer, grown by atomic layer deposition (ALD) at a substrate temperature of 300° C, on n^+ Si(100) covered with an ultra thin oxynitride layer grown in a nitric oxide ambient (no HF-last treatment).[9] More details on the HfO_2 ALD process and the physical and electrical characterization of HfO_2 can be found elsewhere.[10,11] The other sample was a 2.2 nm $Hf_{0.78}Si_{0.22}O_2$ layer grown by MOCVD at 250° C on Si(100) covered with an 0.8 nm SiO_2 interlayer. The samples were outgassed near their deposition temperature for several hours in ultra high vacuum (UHV) in the low 10^{-8} Pa (10^{-10} torr) range to remove volatile surface contaminants, consisting mostly of water. Annealing was done by direct current heating of the ~1.5×7 mm samples, the small size of which facilitated rapid temperature variations in the higher temperature ranges. The temperature was measured with an Impac® IR pyrometer optimized in the 1.45-1.8 μm wavelength range over a sampling spot size of <1 mm. The estimated error was ±10° C.

After the sample cooled to room temperature, it was transferred under UHV to the analysis chamber of a JOEL JSPM 4500A, a variable temperature AFM operating in UHV. All scans were done at room temperature. In the present implementation of the non-contact mode the conductive tip of the cantilever oscillates near its resonance frequency (in the 150-350 kHz range, depending on the cantilever) with amplitude of about ±2 nm and ~2 nm from the surface. The interaction with the surface causes the resonance frequency to shift by an amount $\Delta\omega$ that is proportional to the force gradient (repulsive) F'(z), where z is the surface normal.[5] In normal non-contact AFM operation the topography is traced by keeping $\Delta\omega$ constant by feedback control. Other forces may affect the resonance frequency. In the present case of non-magnetic materials in an UHV environment only electrostatic forces between cantilever tip and the sample are of concern. The force gradient $\partial F_e/\partial z$ of this interaction is added to that of the tip-surface interaction, the feedback reacting under the combined force gradients. The forces arise from electrostatic potentials due to workfunction differences between surface and tip (contact potential difference or CPD), through the application of an external potential V_{ext}, and from localized charge in the sample through image force effects with the tip. In these studies V_{ext} takes the form of a dc bias plus a small low frequency (1 kHz) ac voltage: $V_{ext}=V_b+V_{ac}\sin\omega_p t$. The force gradient takes the form:[6]

$$\partial F_e/\partial z = \tfrac{1}{2}V^2 (\partial^2 C_{eff}/\partial z^2) + \partial F_q(V_{ext})/\partial z = \tfrac{1}{2} [V_b+V_{CPD}+V_{ac}\sin\omega_p t]^2(\partial^2 C_{eff}/\partial z^2) + \partial F_q(V_{ext})/\partial z \quad (1) \equiv F'(z)=F'_{dc} + F'(\omega_p) + F'(2\omega_p),$$

where the frequency dependent terms of interest are:

$$F'(\omega_p)=(\partial^2 C_{eff}/\partial z^2) [V_b+V_{CPD}]V_{ac}\sin\omega_p t + \partial F_q(\omega_p)/\partial z \quad (2)$$

and

$$F'(2\omega_p)=\tfrac{1}{4}(\partial^2 C_{eff}/\partial z^2)V_{ac}^2 \cos(2\omega_p t). \quad (3)$$

$\partial F_q(V_{ext})/\partial z$ is the force gradient acting on the tip, which arises from the interaction of V_{ext} with a localized charge q embedded in a medium with dielectric constant κ. For a spherical tip of radius r and at a distance $\mathbf{d} = z\hat{z} + l\hat{l}$ from the center to the charge, the force gradient is given by

$$\partial F_q(V_{ext})/\partial z=(qV_{ext}r/\varepsilon_{eff})[(l^2-2z^2)/(z^2+l^2)^{5/2}], \quad (4)$$

where l is the lateral distance from the tip apex to the charge and $\varepsilon_{eff}=(\kappa+1)/2$. In eqs. (1-3), C_{eff} is the effective capacitance between cantilever and sample and depends on the geometric details of the system. However, for the close proximity of tip apex to the surface in the present experiments most of the contributions to C_{eff} come from the tip-surface interaction. C_{eff} may be position-dependent across the surface if κ of the dielectric and/or the substrate doping concentration fluctuates laterally. The latter effect modifies the depletion width, but is not expected to be of relevance here for homogeneously doped Si samples. A signal proportional to the fundamental harmonic term (2) is obtained by feeding the demodulated output of the phase-locked amplifier of the AFM detector into a lock-in amplifier tuned at ω_p. The output, which is proportional to V_b+V_{CPD}, is used to generate contrast for a second image that is acquired concurrently with the topography. This image is termed here a Kelvin image. The Kelvin mode allows the freedom of applying an arbitrary bias V_b, which can be used to charge/discharge traps in the dielectric and at the Si interface, as well as provide a means of identifying the polarity of the charge q.[12] The output of the lock-in amplifier can also be compared to a reference, usually 0, and the "error" converted to a variable V_b, which is fed back negatively to maintain zero lock-in output; that is $V_b+V_{CPD}=0$, with V_b corresponding to the negative of the contact potential difference. Contrast in the second image is then generated with the V_b signal, and we term such an image the CPD image. It should be noted that in this mode variations in C_{eff} do not affect image contrast. Both Kelvin and CPD images were acquired in this study. The magnitude of CPD variations in a Kelvin image can be extracted by interpolation of a plot of lock-in output vs. V_b measured in a non-scanning mode under otherwise identical conditions. The contrast scales of the Kelvin images shown here have been converted to a CPD-equivalent representation.

The AFM detector output can also be fed into a second lock-in amplifier tuned to $2\omega_p$. Its output is proportional to the second harmonic term $F'(2\omega_p)$, eq. (3), which contains only contributions from $\partial^2 C_{eff}/\partial z^2$. Thus a third image generated with this signal represents the contribution of C_{eff}. Preliminary findings using this mode will be shown, but the results indicate that the signal is rather weak for the experimental parameters used. To understand this point, we can derive an estimate for the $\partial^2 C_{eff}/\partial z^2$ term with the prior assumption of a spherical tip of radius r located a distance z from the planar surface of a dielectric with relative dielectric constant κ. z is measured relative to the center of the tip. C_{eff} can be obtained by the method of images.[13] Differentiation yields the expression:

$$\partial^2 C_{eff}/\partial z^2 \equiv \sum_{n=1}^{\infty} C_n'' =$$

$$4\pi\varepsilon_o r^{-1} csch\,\alpha \sum_{n=1}^{\infty} [(\kappa-1)/(\kappa+1)]^{n-1}[n^2 csch\, n\alpha\,(1+2csch^2 n\alpha)-csch\, n\alpha\,(scsh^2\alpha+n coth\,\alpha\, coth\, n\alpha)]\,, \quad (5)$$

where $\alpha=cosh^{-1}(z/r)$. Of interest here is the κ-dependent prefactor. It can readily be shown that for a dielectric constant change $\delta\kappa$, the expected variations in the force gradient can be assessed through the expression $\delta C_n''/C_n''=2(n-1)\delta\kappa/(\kappa^2-1)$, which indicates that for the dominant lower terms in the expansion of eq. 5, variations in κ will have limited influence on $\partial^2 C_{eff}/\partial z^2$ and may be largely undetectable for large κ materials.

3. Experimental results for HfO_2

3.1 Interpretation of image features

We will first consider some salient features contained in Kelvin images and their relationship to topographic features. This relationship is more apparent in annealed films because of their more homogeneous composition. Fig.1a and b show the topography and Kelvin image simultaneously taken of a 3 nm HfO_2 film annealed for 1 minute at 750°C in UHV. The topography indicates a nodular morphology of ~10±3 nm in extent composed of smaller ~3 nm features. The dark areas represent depressions, which may or may not be actual physical low points. We have previously established that in SiO_2 gate oxides such low points or "holes" may actually be caused by trapped charge near the surface.[14] The force between such charge and its image in the conductive cantilever tip is attractive, and counters the dominant repulsive force

exerted on the tip by the physical surface. Consequently the electrostatic force gradient is manifested in the topographic image as a hole or depression. The polarity cannot be determined from the topography, but rather from contrast in the simultaneously acquired Kelvin image, shown in Fig. 1b. Because the contrast (black-white scale) is arbitrary, depending on the phase of the lock-in, its relationship to the polarity of the surface potential has to be established experimentally. We have adopted the convention that dark areas in the image are negative relative to the light areas.

A number of dark or negative potential spots in the Kelvin image have corresponding dark areas in Fig. 1a, and they are attributed to negative charge in the near-surface region of the HfO_2 layer. The solid white circles in the figure indicate such a negatively charged area. Further supporting evidence for this interpretation will be presented shortly in conjunction with intensity profiles across the images. More rarely observed are dark spots in the topography that exhibit a light or positive corresponding spot in the Kelvin image; such a case is indicated by the black circles. Frequently it is observed that an extreme contrast feature (either black or white) in the Kelvin image does not correspond to a dark area in the topography, and is therefore not associated with charge, but rather with a CPD or workfunction fluctuation. The dashed oval marks such an area in Fig. 1.

3.2 AFM studies of the as-grown HfO_2 surface

Having established the sort of features and correlation that can be encountered in comparing topography and potential images, we now proceed in analyzing in more detail features of the as-grown and annealed HfO_2 layers. We start with the as-grown films. The topography and Kelvin images for two different bias voltages are shown in Fig. 2. The image pairs were taken sequentially, their location differing only by a small upward drift. Inspection shows the many common features between the two topographic images (a and c) and between the two Kelvin images (b and d), but unlike the images for the annealed sample in Fig. 1, there is little correlation between the topography and Kelvin images in Fig. 2. The latter are dominated less by oxide charge than the annealed sample, but rather by broader potential fluctuations. This point is clarified by looking at cross cuts (profiles) of the topography and potential images taken at the same physical locations, indicated by the dashed lines in Fig. 2. These profiles are shown in Fig. 3, the top pair of curves corresponding to the topography, whereas the two bottom curves represent the corresponding potential profiles. Solid and broken curves are for V_b=0 and –0.7 V, respectively. The topographic profiles show dramatic variations with a change in bias, although many features remain the same. These changes are the consequences of trap charging (height decreases) and discharging (height increases) for the biased situation (broken curve) relative to the unbiased case (solid curve). Generally speaking, high-κ dielectrics and HfO_2 in particular are known to show significantly enhanced charge trapping behavior compared to conventional SiO_2.[15-20] Trap densities of the order of ~10^{12} cm^{-2} are not uncommon. Charge trapping is believed to be due filling of pre-existing traps. New trap creation can occur under certain conditions.[15] Detrapping is also observed in HfO_2 and is found to depend on gate (substrate) bias, temperature and light illumination.[16]

Returning to the profiles in Fig. 3, trap charging is exemplified by a decrease in the center region of the topography profile with increasing negative V_b. A corresponding, rather weak increase is to be noted in the potential profile, which indicates that the potential becomes more positive. A portion of this region is identified by ovals in the images of Fig. 2: the topography clearly shows an increased darkening in 2c compared to 2a, accompanied by a modest brightening in the potential image 2d. The reverse effect is observed in the two wings of the profiles of Fig. 3: the increase in height in the topography corresponds to a modest lowering or increased negative trend in the potential profile. The origin of these effects can be attributed to positive charging of donor-like traps and the discharging of negative or acceptor like traps, which are both located within tunneling distance from the oxide surface, but are otherwise randomly distributed over the oxide surface. An energy band diagram illustrating this point is shown in Fig. 4 for the condition $V_b \approx 0$ (left) and $V_b < 0$ (right).

The potential fluctuations for the two bias cases in Fig. 3 are remarkably similar, except for the just discussed small changes attributed to charging and discharging. This similarity is the consequence of

fluctuations in the CPD, which are not affected by bias changes. The fact that the CPD variations dominate over charge-induced potential variations is a consequence of the dominance of the $V_{ac}\delta V_{CPD}\partial^2 C_{eff}/\partial z^2$ term over the $\partial F_q(\omega_p)/\partial z$ term in eq. (2) for $\delta V_{CPD} \gtrsim 0.03$ V, $\kappa \gg 1$ and for metal coated tip diameters $d_{tip} \gtrsim 10$ nm.[21] We thus conclude from these discussions that the dominant fluctuations in the surface potential for HfO_2 arise from long-range lateral changes in CPD occurring over dimensions of order of tens of nanometer and amplitudes of 0.1-0.2 V for the as-grown HfO_2 sample.

3.3 Force microscopy of the annealed HfO_2 surface

We will discuss here results for a 1 minute 650° C anneal, as those of the 750° C anneal are essentially the same. The results indicate that this treatment crystallized the 3 nm thick HfO_2 layer, in agreement with prior results.[4,9] Fig. 5 depicts the topography and surface potential images for V_b=-0.4 and –1.0 V. The two topographies and their corresponding potential images, which differ only by a small lateral drift, show that they were taken at the same sample location. Less apparent is the correlation between the topography and the Kelvin images, a situation that becomes obvious when one looks at profiles of cross-section cuts along identical paths, such as those indicated by the dashed lines in Fig. 5. These are shown for the topography in Fig. 6a (top) and for the potential in Fig. 6b (bottom). Overall the scans for the two biases look remarkably similar in each panel. Furthermore, the peaks in the topography scan coincide with the valleys in the surface potential scan, as most valleys also coincide with the potential peaks. This correlation, specifically anticorrelation, is in sharp contrast to the as-grown sample of Fig. 3, for which little correlation could be observed between features in the topographic and potential images. Two other differences between the two samples are noted, one the reduced evidence of charging/discharging phenomena in the topography, and secondly, the more regularly undulating topography and surface potential of the annealed sample, with a somewhat smaller "periodicity" of 25-40 nm than for the as-grown sample. It should be noted that a much weaker substructure of 5-10 nm lateral extent is barely apparent in the images. We speculate that the larger quasi-regular features are crystallites formed from the amorphous phase during the anneal. The origin of the potential fluctuations is not known. The peaks in the potential, which are imaged as bright areas, correspond to maxima in the surface potential or workfunction. These peaks correspond to valleys or dark areas in the topography, which are relatively shallow (~0.5 nm) compared to the lateral extent (~30 nm) of the hillocks. The observed workfunction changes are unlikely to arise from differences in crystallite orientations, as such scenario suggests that extreme values in the potentials coincide with maxima in the topography (the approximate center of the crystallites). However, such sites consistently correspond to troughs of the potential fluctuations, which instead show a rather homogeneous value, as seen in Fig. 6b. As the figure indicates, larger fluctuations in the potential are actually observed among the peaks in the potential, which correspond to the troughs in the topography. The troughs are most likely associated with grain boundaries, where fluctuations in composition and structure can be expected, with both variables affecting the local surface potential.

3.4 Summary of image parameters of HfO_2 and comparison with SiO_2.

For comparison purposes, Fig. 7 shows pseudo three dimensional images of the HfO_2 and of a 1.5 nm SiO_2 gate oxide grown on Si(100) by rapid thermal oxidation (RTO) and remote plasma nitridation (PN). The surface texture of the oxides is quite different, although the roughness is comparable, as can be ascertained from the data displayed in the table. It should be reemphasized here, that the measured roughness contains some contributions from the electrostatic effects of random charges. Their contribution is expected to be greater for SiO_2 than it is for the HfO_2 because of the much smaller dielectric constant of SiO_2. In addition, both the smaller κ and the smaller thickness of the SiO_2 layer results in some electrostatic contributions from charge trapped in the interface states.[12] However, such charges produce rather dispersed "holes" in the image which affect the local and mean image roughness, but have a lesser effect on the rms roughness. This is clearly borne out be the data in the table. From the standpoint of roughness and its

implied variations in thickness, the data nevertheless suggests that the roughness of the HfO_2 film compares quite favorably to that of functional SiO_2 gate oxides and consequently should be an acceptable specification. A less clear situation applies to the CPD variations. The as-grown and annealed HfO_2 exhibit CPD fluctuations in line scans in the 0.1-0.25 V range. The fluctuations, however, are larger compared to those of the as-grown SiO_2 sample. Forming gas anneals, which reduce the density of interface states in SiO_2, reduce the CPD fluctuations further.[22]

4. Force microscopy on vacuum annealed $Hf_xSi_{1-x}O_2$

As mentioned in the introduction, the silicates are candidates for high κ gate dielectrics as well, albeit their dielectric constant is lower by almost halve of that of HfO_2. The motivation for their study here is less based on this aspect, but rather by their known instability to high temperature ($\gtrsim$ 750° C) anneals, which result in the formation of separate phases of HfO_2 and SiO_2.[8] Comparable phase separations have also been reported recently for zirconium silicate alloys.[23] It is this feature that we wanted to investigate in order to asses the various contributions to the force gradient, as discussed previously, as well as address issues of sensitivity and resolution. Specifically, we wanted to evaluate the contribution to the capacitance signal $\partial^2 C_{eff}/\partial z^2$ and its relationship to the topography and CPD, a task potentially made simpler because of the drastic differences in the dielectric constant of the separated phases.

The sample used was a 2.2 nm thick $(HfO_2)_{0.78}(SiO_2)_{0.22}$ film grown by MOCVD at a substrate temperature of 250° C on a Si(100) wafer covered with an 0.8 nm SiO_2 buffer layer. The as-grown film was amorphous. After growth, the film was immediately placed in the preparation chamber of the AFM and outgassed for several hours in UHV at ~250° C. For these studies we used two operating modes that were different from the HfO_2 studies discussed above: *i)* the CPD was directly measured by activating the second feed back loop, and *ii)* a second lock-in was used to measure and image the second harmonic signal, which is directly proportional to $\partial^2 C_{eff}/\partial z^2$. When desired, all three images, i.e. topography, CPD and the differential capacitance, can be simultaneously acquired.

Fig. 8 depicts just the topography (a) and the CPD (b) images of the as-grown sample. Although features as small as 3 nm can be identified in the topography, larger sized ones of 10 nm and greater dominate the image, as can be seen in the top profile of inset (c), taken along the dashed line in the image. The corresponding cut through the CPD image is shown below it. Some correlative features between topography and the surface potential can be seen in the images, particularly a striated morphology running in a left-slanted, near vertical direction. However, as can be concluded from the CPD profile in Fig. 8c, there is little or no direct correlation with the surface features of the topography, an observation already made for the amorphous, as-grown HfO_2 film discussed in section 3.2. The deep hole near the 150 nm position has the characteristics of trapped charge near the interface. At the same abscissa value along the cut the CPD signal shows a slight increase, which corresponds to a small reduction in the effective local workfunction. Its sign indicates that it is a positive charge and its modest intensity is consistent with the dominance of the surface potential contributions to the force gradient over those of a charge screened by a high dielectric medium.[24]

The Hf-rich the sample is in an alloy composition range for which rapid thermal annealing in the 700-1000° C range causes separate HfO_2 and SiO_2 phases to nucleate and grow into a random microstructure.[8,25] The results we show here are for a 10 second anneal at 900° C and a subsequent anneal at 10+15 seconds at 1000° C. These were preceded by ten seconds anneals at 50° C step intervals starting at 850° C. Fig. 9 depicts on the left side three images for the 900° C anneal: topography (a) on top, the CPD image (b) in the middle and at the bottom the differential capacitance image (c). Both the topography and the CPD image show enhanced granularity over the as-grown sample images in Fig. 8. Feature sizes in the 5-10 nm dominate, with occasional larger nodules, as can be ascertained from the profile along the indicated cut, which is shown as the top curve in Fig. 10a. The nodular structure and their size distribution is consistent with prior results and suggests that re-crystallization has occurred.[8,25] The CPD image, Fig. 9b,

suggests an implicit similarity with the topography, a correlation that is more apparent in the profiles, of which the CPD profile is shown by the middle curve in Fig. 10a. This curve and the CPD image do not show the smaller, more detailed features of the topography, a decrease in resolution that can be attributed to the longer interaction range of the electrostatic forces. Nevertheless, it can be ascertained that some topographic features in the profiles correspond to CPD minima, for instance the group of topographic peaks near the middle of the profile; some of the other peaks correlate with peaks in the CPD profile.

The results thus far suggest the existence of different phases in the annealed film. Their chemical identity cannot be ascertained by the techniques used here. However, a possible indicator of a κ-dependent differentiation may be possible by looking at the differential capacitance, which should directly correlate with the value of the dielectric constant, provided that capacitance changes are not dominated by roughness in the topography. The rms roughness of this sample was only 0.077 nm, an excellent value when comparing it to those summarized in Fig. 7. The differential capacitance image is shown in Fig. 9c, and the profile along the previously described cuts is shown by the dotted lower curve in Fig. 10a. As eq. 3 indicates, the prefactor and the square of the applied bias are expected to make this signal weak for the low V_{ac} values used here, which accounts for the faded appearance of the differential capacitance image. Nevertheless, the profile exhibits considerable structure of high and low differential capacitance. Moreover, the peak positions, corresponding to high differential capacitance, correlate frequently with peaks in the topography. This indicates that topographic features are not the dominant contributors to capacitance changes here, for otherwise the high topographic feature would diminish rather than increase the differential capacitance, as observed. We thus suggest that the increases in differential capacitance are due to inreases in dielectric constant, which supports the notion of a phase separation into low and high κ material, the lower values presumably corresponding to SiO_2-related material and the others to HfO_2.

A different perspective of the interplay of structure, surface potential and capacitance can be garnered from the AFM images of the 25 second anneal at 1000° C, shown in the right panel of Fig. 9. The anneal in ultra high vacuum results in the decomposition of the already phase separated former silicate layer into HfSi and SiO_2, in analogy to what occurs with Zr compounds on Si.[26] It should be pointed out that the silicide formation is inhibited when the anneal occurs in an environment containing trace amounts of oxygen or if the hafnium silicate layer is capped with a polysilicon layer.[27] The silicide, which is metallic, forms rather large nodules in direct contact with the Si substrates. Its composition was confirmed by XPS.[28] The topographic image of this phase is shown in Fig. 9d. It is the result of a second 15 second anneal at 1000° C after the prior 10 second anneal at 1000° C resulted in but a modest enhancement of the roughness compared to that of the 900° C anneal.[29] The nodular features range in lateral extent from ~7 to 35 nm, with the larger sizes dominating. The height profile of the cut along the dashed line in Fig. 9d is shown by the dashed curve in Fig. 10b. Many of the larger nodules are of fairly uniform height, extending up to ~4 nm above the background plane. Some of the nodules exhibit compounded structures that appear to be made up of different compositions or are covered with a layer of different surface potential, as can be ascertained from the corresponding features in the CPD image shown in Fig. 9e. The potential profile along a cut of coordinates identical to those for the topography profile is shown by the solid line in Fig. 10b. It indicates that the inter-nodular region exhibits a fairly uniform CPD, whereas the segments corresponding to the nodules exhibit CPD's of essentially bimodal values lower by ~0.1 and ~0.3 V. This bimodal distribution is also quite evident in the CPD image (Fig. 9e), but clearly absent in the differential capacitance image, shown in Fig. 9f, which shows the nodules as exhibiting a uniform differential capacitance that is lower (darker) than that of the inter-nodular region. The profile along the dashed line matching those of the topography and CPD images is shown by the dotted curve in Fig. 10b. It shows that the differential capacitance minima correspond to the pronounced maxima in the topography. The comparison also indicates a direct correspondence of high capacitance with high CPD's, although some, primarily the secondary minima in the CPD profile, still correspond to maximum or near maximum values in the capacitance. We interpret the results in terms of pinning of the interface Fermi level beneath the silicide nodules, a process that adds serial capacitance due to an increased depletion width in the Si, thereby

lowering the effective capacitance sensed by the tip. The inter-nodular region, covered with the remnant of the SiO_2 layer exhibits a higher capacitance because of the expected lower density of interface states.

5. Concluding remarks

The objective of this work was an evaluation of certain physical and material properties of Hf-based compounds in order to assess their suitability as high-κ substitutes for SiO_2-based gate stacks. The experimental techniques were force microscopy methods based on the non-contact AFM mode operating in UHV, which allow not only a high resolution topographic assessment of the surface roughness, but also the mapping of surface potential variations and differential capacitance arising from compositional fluctuations. However, the technique, because of a present lack of a materials-sensitive spectroscopic mode, does not yield direct chemical information. Nevertheless the important issues of surface roughness, compositional homogeneity, as expressed through the surface potential maps, and some aspects of dielectric constant variations through capacitance changes could be addressed. A specific goal was the evaluation of the film characteristics following various annealing steps, unavoidable procedures in device fabrication, that lead to profound changes in composition, morphology and crystalline order. We observed that the as-grown and annealed HfO_2 and $Hf_{0.78}Si_{0.2}O_2$ layers essentially retained their smoothness even after undergoing crystallization and that the measured roughness compares favorably to state-of-the-art RTO and nitrided SiO_2 gate oxides. Surface potential variations, obtained by direct measurement of the contact potential difference, were of the order of 0.3-0.4 V on an image-wide basis (and about half this range on a local scale), a magnitude that did not change appreciably with the anneals. A lack of correlation between topographic and CPD image features for the as-grown amorphous samples changed dramatically once the films crystallized, with higher CPD values corresponding to the grain boundary regions for both the oxide and silicate layers. We have no explanation for this behavior, although we can exclude trapped charge as a dominant mechanism. Charge trapped near the surface of the layer had almost negligible effects on the surface potential in these high κ materials, an observation that is supported by model calculations. The magnitude of the CPD fluctuation was higher by about a factor of two than those observed for SiO_2. As their lateral extent in the tens of nanometer range is much larger than the electron wavelength, diffuse scattering of the electrons and an associated mobility degradation does not seem to be a concern. However, as future channel lengths begin to approach these dimensions, such variations may lead to variations in threshold voltages along the channel width. The results of the differential capacitance measurements imply that at present only large dielectric constant variations can be detected. Modeling of the tip-dielectric surface interaction, however, indicates that other than subtle κ variations, particularly for $\kappa \gtrsim 15\text{-}20$, will be difficult to differentiated without drastic improvement in instrumental sensitivity and resolution. It was also determined that a low surface roughness was essential to observe κ-dependent features in the differential capacitance images. In its present implementation, the differential capacitance can nevertheless be a useful technique in conjunction with the other imaging methods to differentiate among possible mechanisms of image contrast, as was demonstrated here for the annealed $Hf_{0.78}Si_{0.2}O_2$ samples.

Acknowledgement: special thanks to Matt Copel for MEIS and XPS measurements and Ed Cartier and Max Fischetti for many useful discussions.

References

1. G. D. Wilk, R. M. Wallace, J. M. Anthony, J.Appl.Phys., **89**, 5243 (2001).
2. M. L. Green, E.P. Gusev, R. Degrave, and E. Garfunkel, J. Appl. Phys. **90**, 2057 (2001).
3. S. Guha, E. P. Gusev, M. Copel, L-Å. Ragnarsson, and D. A. Buchanan, MRS Bulletin **27,** 226 (2002).
4. M.-Y. Ho, H. Gong, G. D. Wilk, B. W. Bush, M. L. Green, W. H. Lin, A. See, S. K. Lahiri, M. E. Loomans, P. I. Räisänen and T. Gustafsson, Appl. Phys. Lett. **81**, 4218 (2002).
5. T. R. Albrecht, P. Grütter, D. Horne and D. Rugar, J. Appl. Phys. 69, 668 (1991).
6. M. Nonnenmacher, M. P. O'Boyle and H. K. Wickramasinghe, Appl. Phys. Lett. **58**, 2921 (1991).
7. S. Kitamura and M. Iwatsuki, Appl. Phys. Lett. 72, 3154 (1998).
8. S. Ramanathan, P. C. McIntyre, J. Luning, P. S. Lysaght, Y. Yang, Z. Chen and S. Stemmer**,** J. Electrochem. Soc. **150,** F173 (2003).
9. E. P. Gusev, C. Cabral Jr., M. Copel, C. D'Emic, and M. Gribelyuk, Microelectronic Engineering **69**, 145 (2003).
10. K. Kukli, M. Ritala, J. Sundqvist, J. Aarik, J. Lu , T. Sajavaara, M. Leskelä and A. Hårsta, J. Appl. Phys.**92**, 5698 (2002).
11. G. D. Wilk and D. A. Muller, Appl. Phys. Lett., 83, 3984 (2003).
12. R. Ludeke and E. Cartier, Appl. Phys. Lett. **78,** 3998 (2001).
13. W. R. Smythe, Static and Dynamic Electricity, 2nd Edition, McGraw-Hill, New York, 1950, p.121. and J. D. Jackson, Classical Electrodynamics, John Wiley, NY 1962.
14. R. Ludeke, J. Non-crystalline Solids, **303**, 150 (2002).
15. A. Kumar, T.H. Ning, M.V. Fischetti and E. P. Gusev, J. Appl. Phys. **94**, 1728 (2003).
16. E. P. Gusev and C. D'Emic, Appl. Phys. Lett. **83,** 5223 (2003).
17. S. Zafar, A. Callegari, E. P. Gusev, and M.V. Fischetti, , J. Appl. Phys. **93**, 9298 (2003).
18. M. Houssa, M. Naili, M. M. Heyns and A. Stesmans, J. App. Phys. **89**, 792 (2001).
19. A. Kerber, E. Cartier, G. Groeseneken, H. E. Maes and U. Schwalke, J. Appl. Phys. **94**, 6627 (2003).
20. Wei He and T. P. Ma, Appl. Phys. Lett. **83**, 5461 (2003).
21. For the experimental conditions and ΔV_{CPD}=0.2 V, the first 5 terms of eq. 5 were used to estimate the ratio of capacitive and charge contribution to the force gradient: $\Delta V_{CPD} V_{ac} \partial^2 C_{eff}/\partial z^2 / \partial F_q(V_{ac})/\partial z \approx 40$. A single electron charge near the surface of the oxide and directly under the tip (l=0) was used for the $\partial F_q(V_{ac})/\partial z$ term (eq. 4). It is worth noting that for SiO_2 (κ=3.9) these two terms are comparable.
22. R. Ludeke and E. Cartier, unpublished results: the CPD image roughness of a 1.8 nm SiO_2 film on n-type Si(111) in ref. 12 improved ~60% when the interface state density of 5×10^{12} cm^{-2} was reduced by over an order of magnitude by a forming gas anneal.
23. G. B. Rayner, Jr., D. Kang, and G. Lucovsky, J. Vac. Sci. Technol. B **21**, 1783 (2003).
24. The polarity of the V_{CPD} bias is referenced to the tip, whereas V_b, which was used in the Kelvin images to obtain contact potential changes, is referenced to the substrate.
25. S. Stemmer, Y. Li, B. Foran, P. S. Lysaght, S. K. Streiffer, P. Fuoss and S. Seifert, Appl. Phys. Lett. **83**, 3141 (2003).
26. M. A. Gribelyuk, A. Callegari, E. P. Gusev. M. Copel and D. A. Buchanan, J. Appl. Phys. **92**, 1232 (2002).
27. P. S. Lysaght, unpublished results.
28. M. Copel, private communications.
29. R. Ludeke, unpublished results.

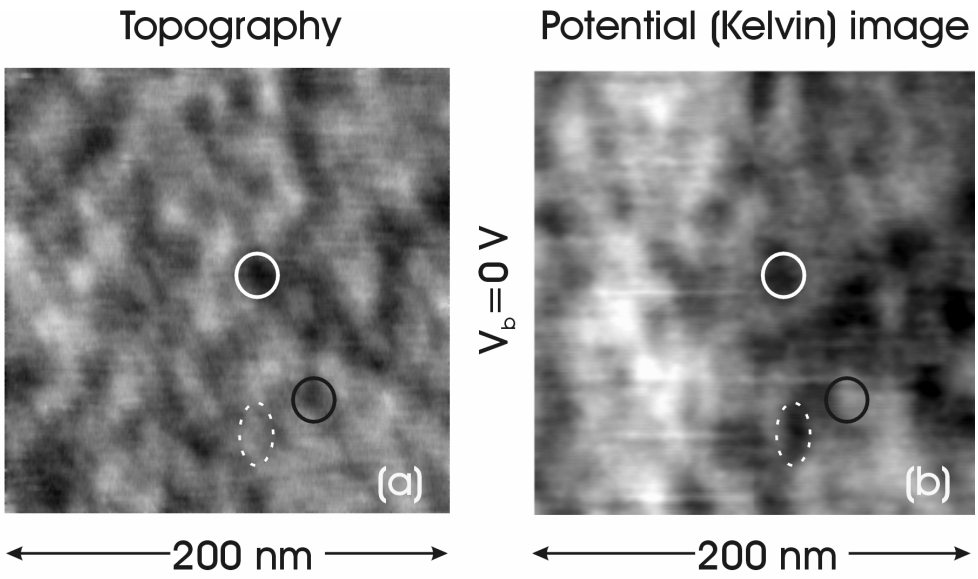

HfO30a20t&k HfOpap Fig. 1

Fig. 1. 200 nm^2 topography (a) and surface potential (Kelvin) image (b) of a 3 nm HfO_2 layer annealed at 750° C for 1 minute. White (black) circles mark trapped negative (positive) charge in the immediate surface region. See text for further details. Black-white image contrast: a) 0.89 nm; b) 0.45 V.

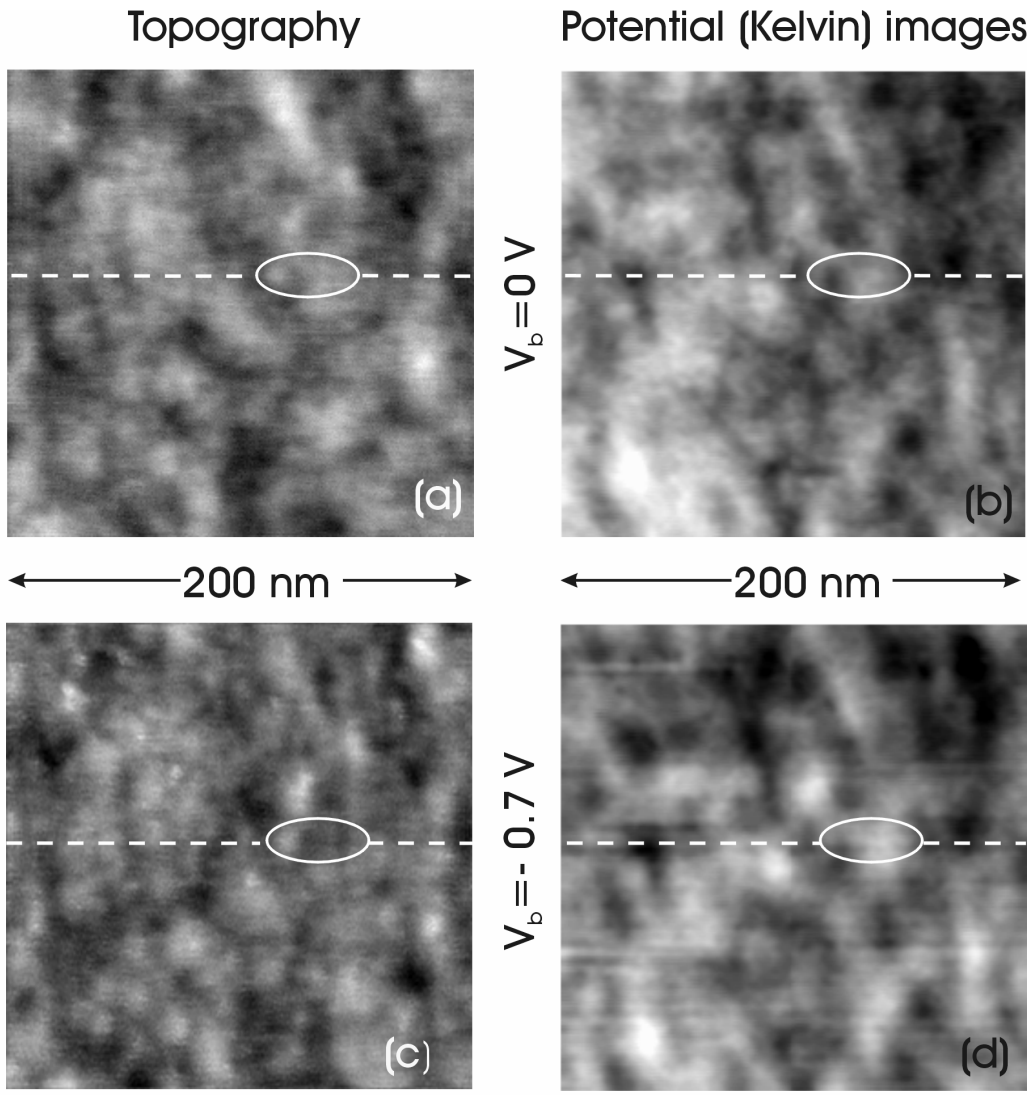

HfO30u01,02t&k HfOpap Fig.2

Fig. 2. 200 nm^2 topography, (a) and (c) and Kelvin images (b) and (d) for an as-grown 3 nm HfO_2 layer for V_b=0 (a and b) and V_b=-0.7 V (c and d). Dashed lines mark cuts where image intensity profiles, shown in Fig. 3, were measured. Black-white image contrast: a) 0. 95 nm; b) 0.42 V; c) 1.1 nm; d) 0.44 V.

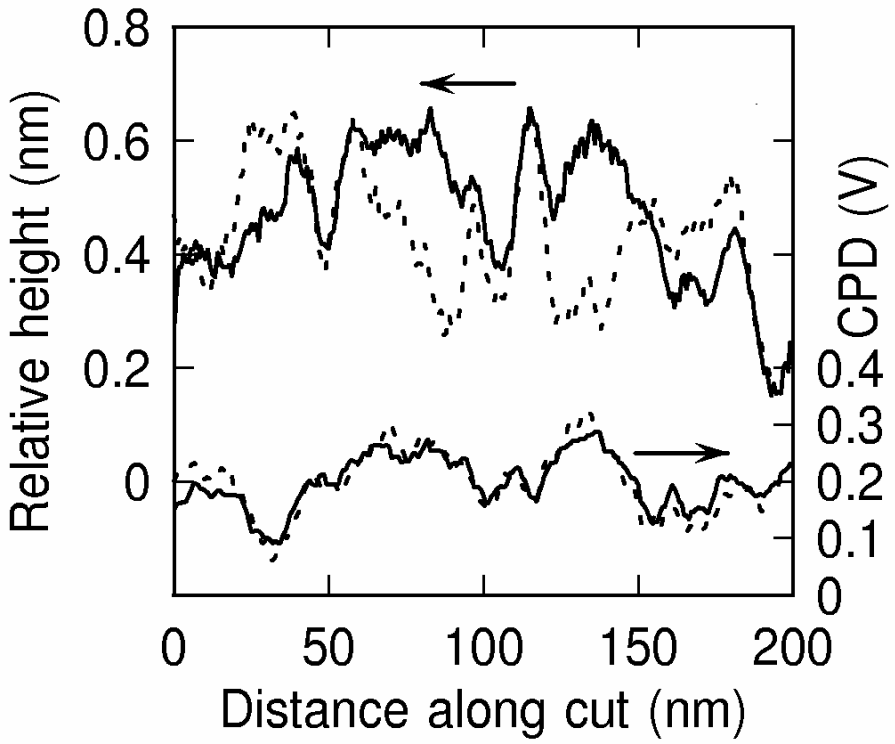

Fig. 3. Image intensity profiles along cuts indicated in Fig. 2 for as-grown 3 nm HfO_2 layer. Top pair represents the topographic or height changes, bottom pair the surface potential changes. Solid lines are for V_b=0, dotted lines for V_b=–0.7 V.

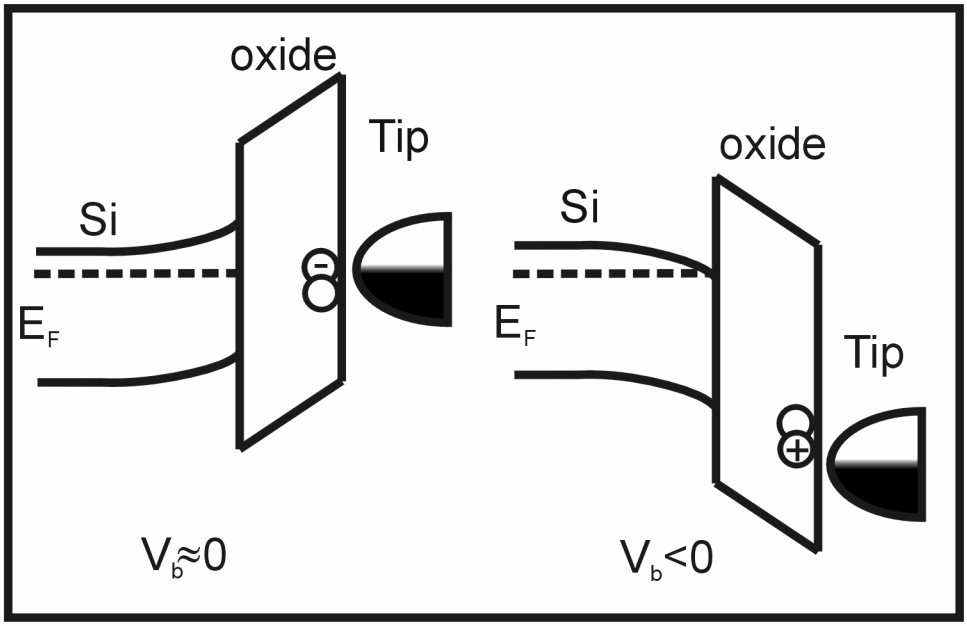

HfOpap Fig. 4

Fig. 4. Schematic view of tip-sample band line up for near zero and negative sample biases. The circles represent charge traps near the surface opposite the AFM cantilever tip. The tip induced band bending causes charge to be transferred between sample and tip. The sign indicates the polarity. An open circle represents the neutral state.

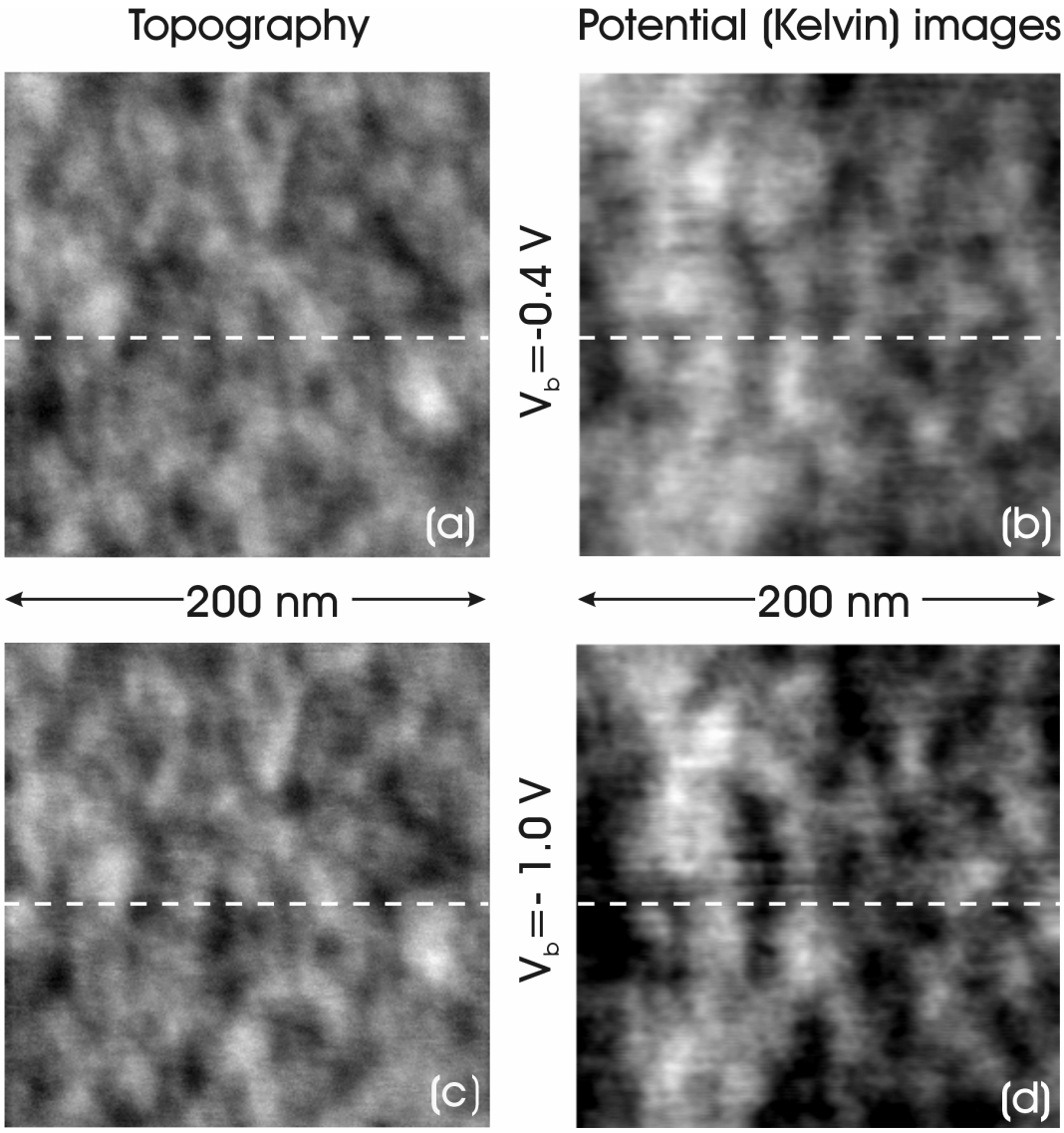

HfO30a08,10t&k HfOpap Fig.5

Fig. 5. 200 nm^2 topography, (a) and (c) and Kelvin images (b) and (d) for the 3 nm HfO_2 sample annealed for 1 min. at 650° C. Images were taken at V_b=−0.4 V (a and b) and V_b =−1.0 V (c and d). Dashed lines mark cuts where image intensity profiles, shown in Fig. 6, were measured. Black-white image contrast: a) 1.0 nm; b) 0.37 V; c) 0.98 nm; d) 0.35 V.

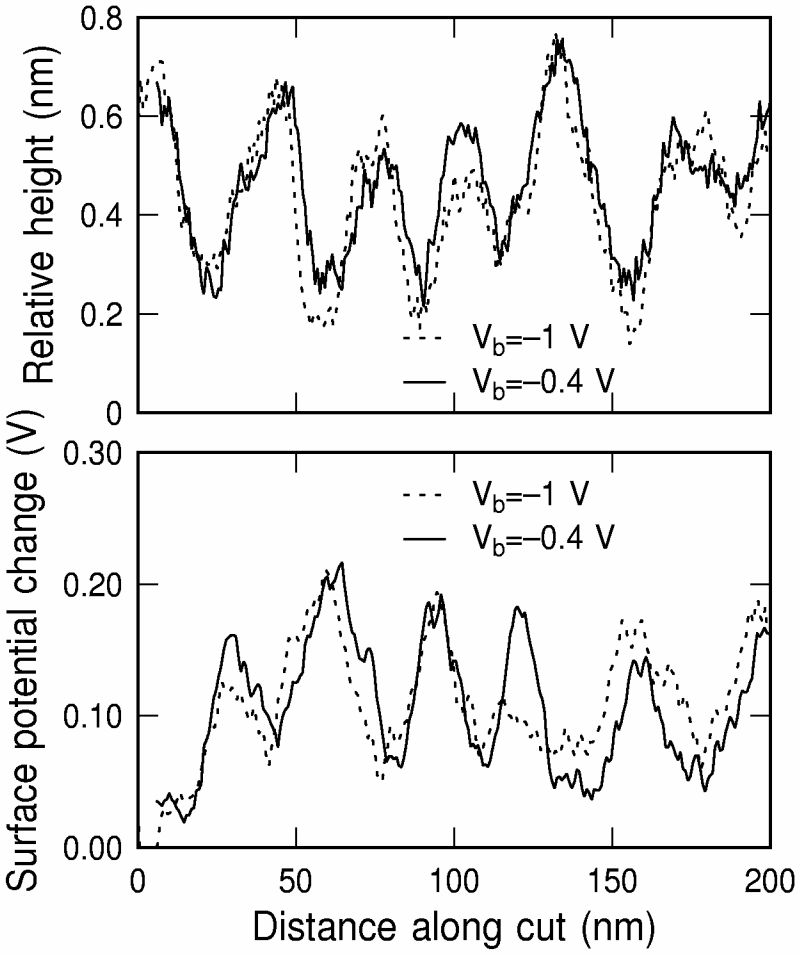

Fig. 6. Image intensity profiles along cuts indicated in Fig. 5 for annealed 3 nm HfO_2 layer. Top panel shows the topographic or height changes, bottom panel the surface potential changes. Solid lines are for V_b=−0.4 V, dotted lines for V_b=−1.0 V.

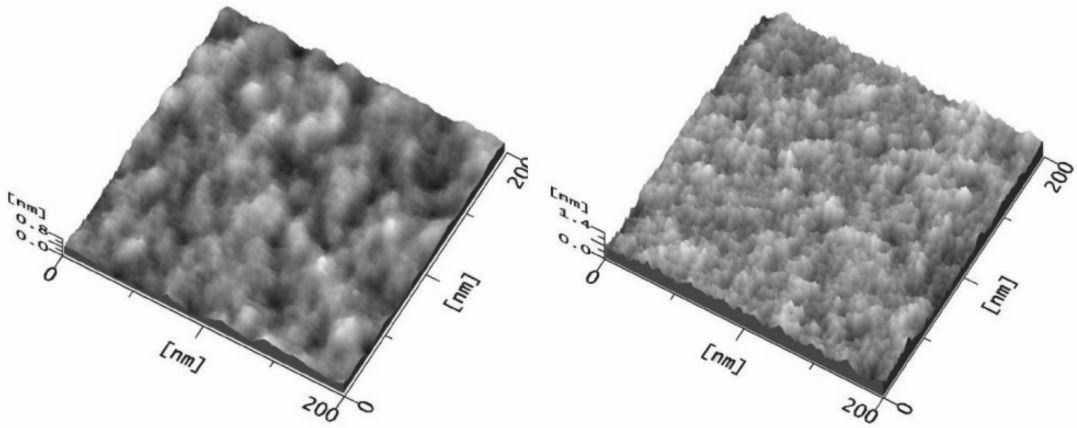

3 nm ALD HfO_2 annealed 1.5 nm RTO/PN SiO_2

Sample	mean image roughness (nm)	RMS image roughness (nm)	"local" peak-to-valley roughness (nm)	CPD peak-to-valley range (V)
HfO_2 3 nm ALD	0.441	0.137	0.3-0.4	0.1-0.2
+ 650°C anneal	0.464	0.140	0.3-0.4	0.1-0.2
+ 750 °C anneal	0.443	0.128	0.3-0.4	0.1-0.25
RTO SiO_2 + PN	0.5-0.8	0.11-0.13	0.5-0.8	0.08-0.14

HfOpap Fig 7

Fig. 7. Images of annealed 3nm HfO_2 and a 1.5 nm nitrided RTO SiO_2 film. Their characteristics are listed and compared in the table below the images. Note that the CPD ranges are given for line scans and differ from those in Figs. 2 and 5, which are quoted for the entire image.

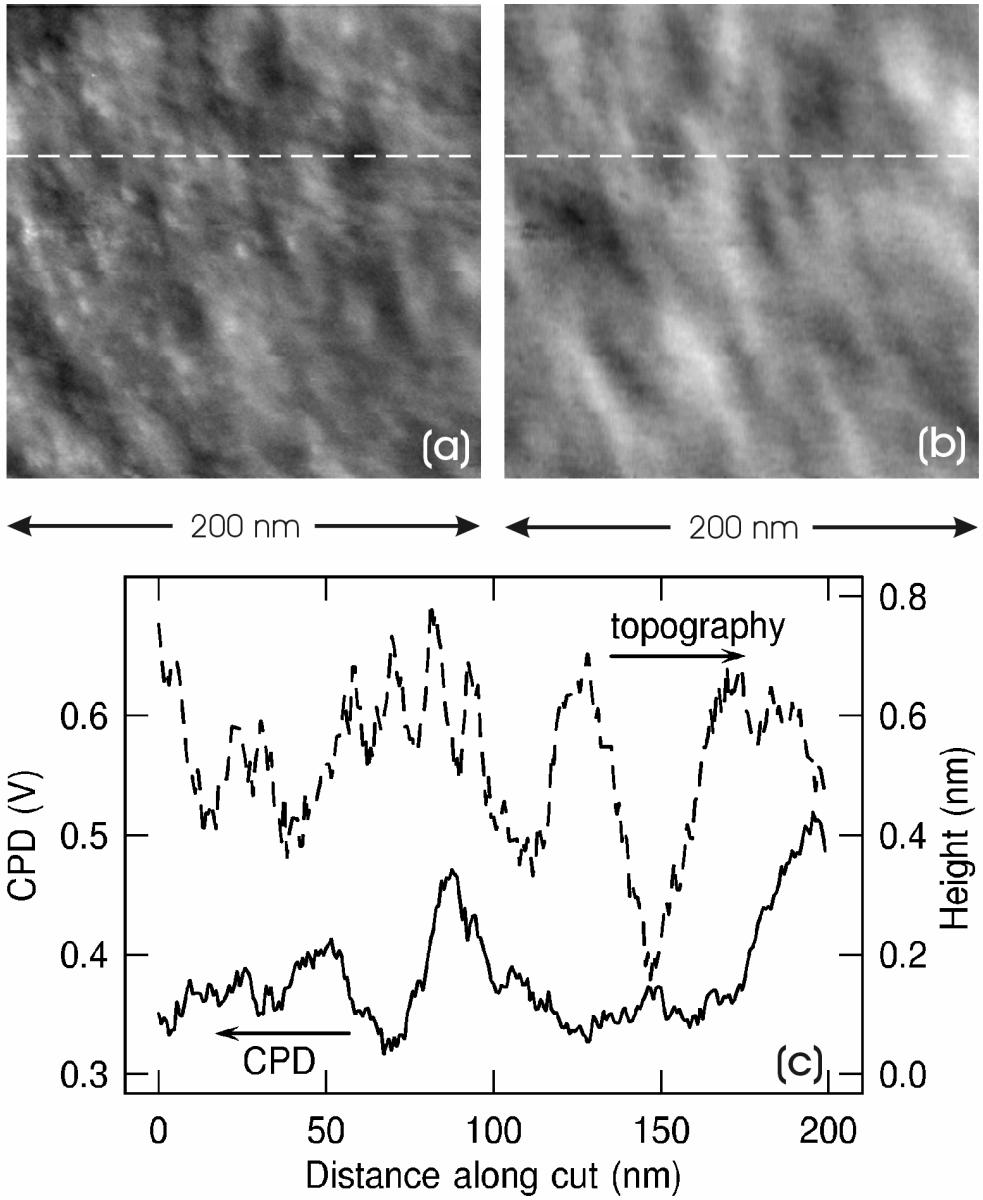

HfOpap Fig. 8

Fig. 8. 200 nm^2 topography, (a) and CPD image (b) for as-grown 2.2 nm $Hf_{0.78}Si_{0.22}O_2$ layer. Dashed lines mark cuts where image intensity profiles, shown in (c), were measured. Black-white image contrast: a) 1.2 nm; b) 0.38 V.

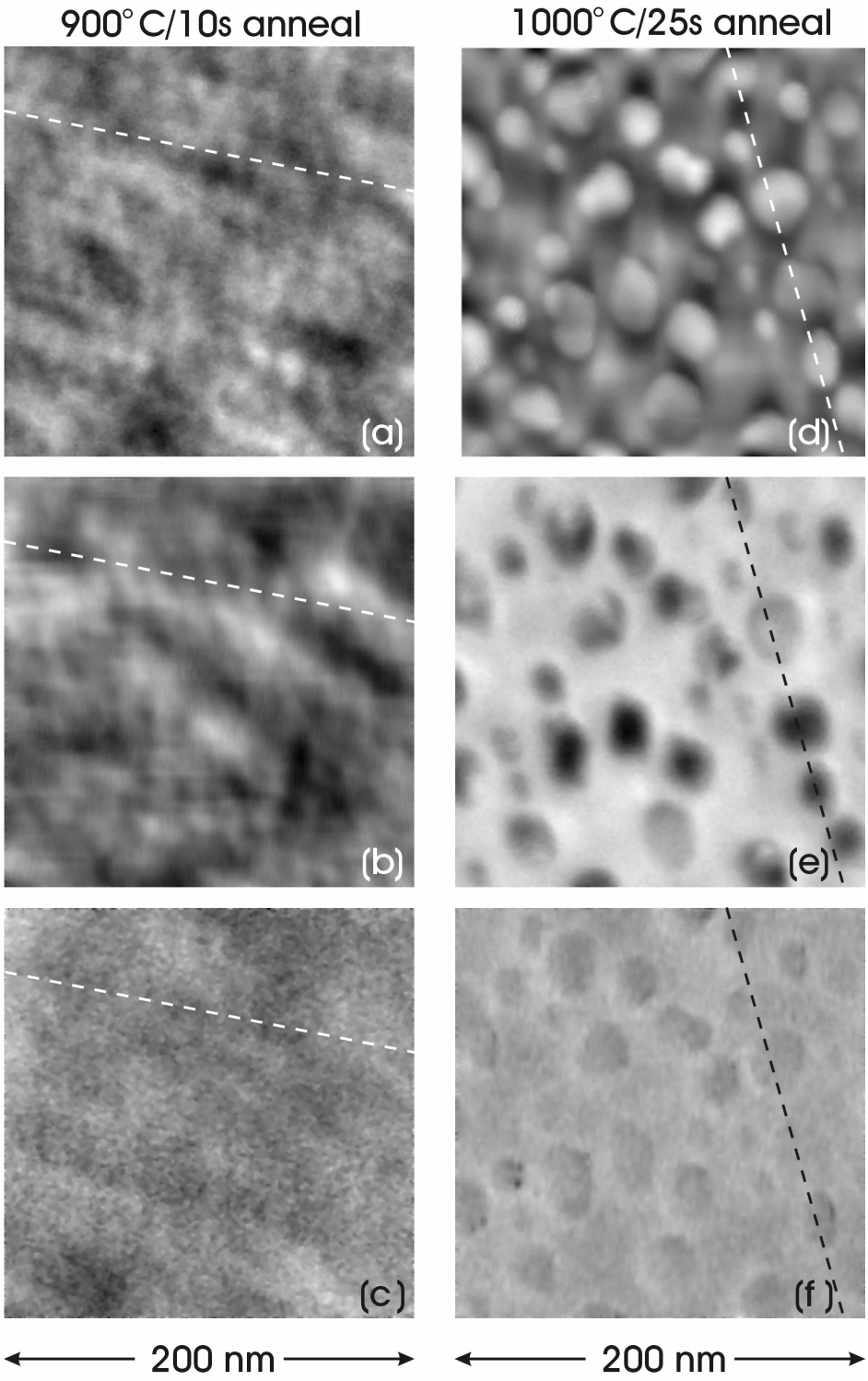

HfOpap Fig. 9

Fig. 9. 200 nm^2 topography (a and d), CPD (b and e) and differential capacitance (cand f) images for 2.2 nm $Hf_{0.78}Si_{0.22}O_2$ layer annealed for 10 seconds at 900° C (left panel) and for 25 seconds at 1000° C (right panel). Dashed lines mark cuts where image intensity profiles, shown in Fig. 10, were measured. Black-white image contrast: a) 0.624 nm, (0.077 m rms roughness); b) 0.21 V; d) 9.1 nm (0.58 roughness); e) 0.50 V.

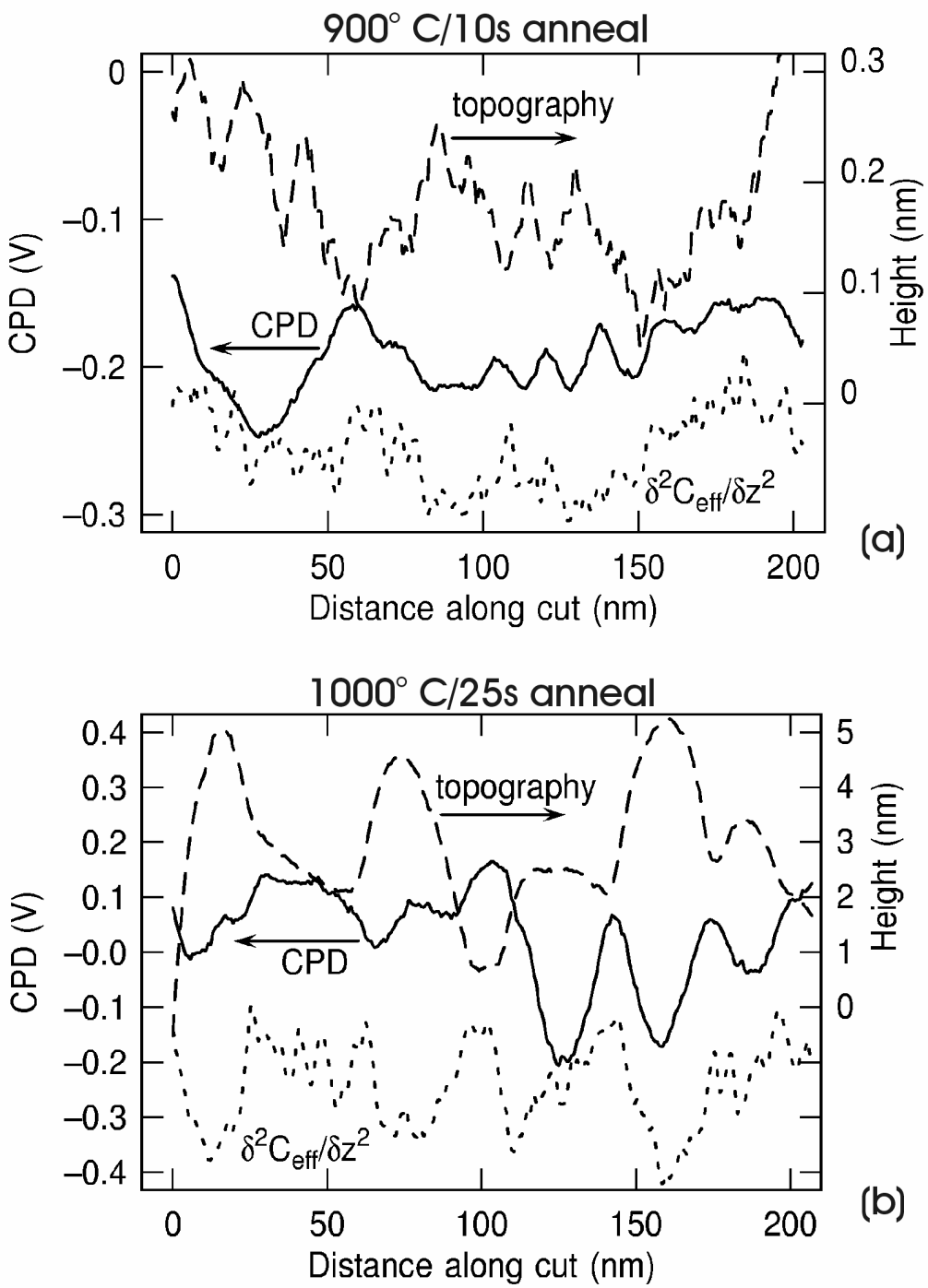

HfOpap Fig.10

Fig. 10. Image intensity profiles along cuts indicated in Fig. 9 for 2.2 nm $Hf_{0.78}Si_{0.22}O_2$ layer annealed for 10 seconds at 900° C (panel a) and for 25 seconds at 1000° C (panel b). Topography changes are indicated by dashed lines, CPD changes by the solid lines and changes in differential capacitance by dotted lines. Note that the latter have no ordinate scales, as the output of the corresponding image channel is not calibrated.